Biosensors and Bioelectronics 143 (2019) 111622

Contents lists available at ScienceDirect

Biosensors and Bioelectronics

journal homepage: www.elsevier.com/locate/bios

Mussel-inspired enzyme immobilization and dual real-time compensation algorithms for durable and accurate continuous glucose monitoring

Kwang Bok Kim[a,1], Hyoungseon Choi[b,1], Hyun Joo Jung[b], Young-Jae Oh[b], Chul-Ho Cho[b], Jin Hong Min[b], Seoyoung Yoon[b], Jaepil Kim[b], Seong Je Cho[b,**], Hyung Joon Cha[c,*]

[a] Biomedical System and Technology Group, Korea Institute of Industrial Technology, Cheonan, 31056, South Korea
[b] Samsung Research, Samsung Electronics, Seoul R&D Campus, Seoul, 06765, South Korea
[c] Department of Chemical Engineering, Pohang University of Science and Technology, Pohang, 37673, South Korea

ARTICLE INFO

Keywords:
Continuous glucose monitoring
Electrochemical sensor
Glucose oxidase immobilization
Mussel adhesive protein
Real-time compensated algorithm
Clinical evaluation

ABSTRACT

Blood glucose sensing is very important for diabetic management. It is shifting towards a continuous glucose monitoring because such a system can alleviate patient suffering and provide a large number of glucose measurements. Here, we proposed a novel approach for the development of durable and accurate enzymatic continuous glucose monitoring system (CGMS). For the long-term durable and selective immobilization of glucose oxidase on a microneedle electrode, a biocompatible engineered mussel adhesive protein was employed through efficient electrochemical oxidation strategy. For the accurate performance in *in vivo* environments, we also suggested dual real-time compensated algorithms to cover both temperature and time-lag differences. After preclinical and pilot-clinical evaluations, we confirmed that our proposed CGMS has an outstanding performance compared with various commercially available continuous systems and achieves comparable performance to disposable glucose sensors.

1. Introduction

Diabetes mellitus is increasing worldwide at an unprecedented pace: the number of diabetic patients was estimated to be approximately 171 million in 2000, and it is expected to reach 552 million by 2030 (Whiting et al., 2011). Recently, the trend in blood glucose management is shifting towards a continuous glucose monitoring system (CGMS) (Shi and Hu, 2014). CGMS alleviates diabetic suffering for those who have to frequently prick their finger. CGMS provides a large number of glucose measurements, which are highly useful for healthcare professionals, who can determine the fasting and postprandial blood glucose levels and better adjust the insulin dose and can detect unrecognized hypo- or hyper-glycemia (Guillod et al., 2007). However, the commercially available CGMSs have not only a relatively long needle causing pain and discomfort but also a lower accuracy than disposable systems (Rodbard, 2016). In addition, due to the high maintenance expenditure, patients are reluctant to use CGMS. Thus, many researchers are struggling to overcome these issues.

Unlike disposable glucose monitoring systems, the CGMS sensor must maintain sensitivity for several days under the human skin. Strategies for enhancing the repeatability and stability of the glucose sensor have been studied on an immobilizing mediator and with the glucose oxidase (GOx) enzyme (NIRAJ et al., 2012). The mediators, which have a lower oxidation potential, facilitate electron transfer by rapidly shuttling electrons between the enzyme and electrode (Carr and Browers, 1980; Linke et al., 1994). For a high sensitivity and stability of the glucose sensors, chemical attachment and entrapment of the mediator and enzyme have been used (Bartlett and Blrkln, 1994; Battaglinit and Calvo, 1994; Cass et al., 1984; Harkness et al., 1993; Lion-Dagan et al., 1994; Schmidt et al., 1993; Yoneyama and Kajiya, 1993). The immobilized mediator and enzyme are coated with biocompatible protective membranes, such as phosphorylcholines (Yang et al., 2000), polyurethane with phospholipids (Ishihara et al., 1996), and hydrogels (Suri et al., 2003), to minimize the biofouling and immune response. Although minimally invasive CGMS technologies have more robust selectivity, sensitivity, and enhancing stability than they have previously had, they have a limitation in prolonging the lifetime of the sensor in the human body (Vashist, 2013). Therefore, it is important to maintain the enzyme activity under an aggressive biological environment, including proteins, lipids, and interference, to achieve long-term

* Corresponding author.
** Corresponding author.
E-mail addresses: seongje.cho@samsung.com (S.J. Cho), hjcha@postech.ac.kr (H.J. Cha).
[1] Kwang Bok Kim and Hyoungseon Choi contributed equally to this work.

https://doi.org/10.1016/j.bios.2019.111622
Received 24 July 2019; Received in revised form 16 August 2019; Accepted 20 August 2019
Available online 23 August 2019
0956-5663/

use.

After inserting the sensor into the skin, the external environment where the sensing needle is placed, including its temperature and time-lag, must be considered (Singh and Verma, 2013; Sinha et al., 2017). Because the protein structure is sensitive to temperature, the rate of an enzyme-catalyzed reaction fluctuates with the skin temperature (Szasz, 1974). At a low temperature, the rate of the reaction is low, and *vice versa*. Therefore, in an enzyme-based glucose sensor, temperature compensation is essential for high accuracy. In addition, the sensor of a CGMS measures the glucose concentration in ISF, unlike disposable glucose sensors, which do so in the blood (Vashist, 2013). Several studies demonstrate that the equilibrium of the glucose concentration across the capillary endothelial membrane is not spontaneous (Rebrin and Steil, 2000; Steil et al., 2005). As a consequence, there is a time-lag phenomenon between the ISF glucose and blood glucose, in which the ISF glucose lags behind the blood glucose (Stout et al., 2004). According to many studies on time-lag, the estimated time-lag ranges from 5 min to 40 min in human subjects (Schmelzeisen-Redeker et al., 2015). Therefore, the physiological time-lag of the CGMS measurements should be mitigated for high accuracy and hypo/hyperglycemic alerts.

In this work, we introduced an innovative solution for enzyme immobilization on the surface of a microneedle electrode that uses bioengineered mussel adhesive protein (MAP). MAPs are known as potential biomedical and environmentally friendly underwater bioadhesives due to their strong and flexible adhesion with substrate-independent manner (Cha et al., 2008). Most importantly, their adhesion is maintained even in wet environments, e.g., *in vivo*, while chemical adhesives are easily weakened or broken by water (Cha et al., 2008; Yang et al., 2016). MAPs have a higher proportion of 3,4-dihydroxyphenylalanine (dopa) residue, which is catecholic amino acid produced by the post-translational hydroxylation of tyrosine (Cha et al., 2008). 3,4-Dihydroxyphenyl (catechol), a side chain of the dopa residues, plays a key role in forming strong hydrogen bonds with the electrode surfaces (Maleki et al., 2012). Moreover, dopa residues enable MAPs to cross-link each other *via* the oxidative conversion to dopaquinone (Yu et al., 2011). In addition, we suggested new compensation algorithms to improve the performance of the proposed CGMS by reducing the temperature effects and time-lag between ISF glucose and blood glucose.

2. Materials and methods

All the materials, reagents, experimental methods, and instrumentations used throughout this study are described in detail in the Supporting Information.

3. Results and discussion

3.1. Fabrication of glucose sensor

The carbon layer, as a working electrode, and the Ag/AgCl layer, as a counter electrode, were silk-screen printed on a polyethylene terephthalate (PET) film at the top and bottom (Fig. 1a). The CO_2 laser cut the PET film into a needle shape with a height and width of 1.5 mm and 700 μm, respectively. To increase the efficiency of the electron transfer from the GOx enzyme to the electrode, the ferrocene carboxylic acid layer, as an electron-transfer mediator, was electrodeposited on the carbon electrode (Atta et al., 2012; Hamad et al., 2014). The ferrocene carboxylic acid (10 mM) was dissolved in 100 mM TBAP in acetonitrile, and the needle electrode was then dipped in the solution. The electrodeposition was done by applying 25 repeated cycles in a potential range (−0.2 V–1.2 V) versus Ag/AgCl, which was washed with 100 mM phosphate buffer (pH 7.4) under an applying potential from −0.1 V to 0.6 V (15 cycles). Then, the mediator-modified electrode was immersed in distilled water for 10 min and dried at room temperature for 1 h.

Dopa and dopamine, a decarboxylation product of dopa, have been widely investigated as a polymer matrix that forms *via* spontaneous oxidation and cross-linking for use in surface engineering and biological applications because of their intrinsic biocompatibility and strong adhesive forces (Xi et al., 2009). They have also been used as biosensor elements and connecting materials for biomolecules, such as proteins and DNAs (Chao et al., 2013; Zhang et al., 2015). However, the oxidation process takes such a long time that it generates many side products, which do not participate in polymer matrix formation (Lee et al., 2007, 2009). Electrochemical biosensors can cause a short-circuit between the working and reference electrodes. Therefore, for the fast and selective immobilization of GOx molecules on an electrode, our novel approach was to electrochemically oxidize the dopa residues of MAP (Fig. 1b). Here, dopa-incorporated foot protein-3 (fp-3) MAP was chosen as a polymer matrix (Yang et al., 2014). The optimal reaction conditions, such as an acidic environment, the concentration, the mixing ratio, the potential range, and the number of cycles in cyclic voltammetry, were determined to maximize the sensitivity and reproducibility of the sensors. Then, 2 mg mL^{-1} MAP and 200 mg mL^{-1} GOx were dissolved in 10 mM acetate buffer (pH 4). The mixture of MAP and GOx was electropolymerized on the working electrode of the micro-needle sensor through a potential cycling from −0.3–0.7 V (vs. Ag/AgCl) at a scan rate of 100 mV s^{-1} (Fig. 1c). We found that an even enzyme layer was formed through the reaction of the electrochemically oxidized dopaquinones of MAP with amines or thiols of GOx, whereas a rough spontaneously oxidized layer was formed using the same mixture in an ambient condition (Fig. S1). The rough interface between the electrode and enzyme can lower the conductivity, causing the sensitivity and reproducibility of sensors to deteriorate. In contrast, the even and flat interface can contribute to a smooth electron flow between them and help enhance the sensitivity. The electrochemical oxidation had many advantages over the spontaneous oxidation. First, it shortened the reaction time remarkably; only several minutes were required for the entire electrochemical process. The oxidation of the MAP molecules and the covalent bonding with the GOx enzymes occurred simultaneously in one step. Second, only the electrochemically potential-applied area was selectively oxidized. This meant that we controlled where the enzymes covered. The reference electrodes were also prevented from being affected by the sensor fabrication process, and a short circuit was avoided. Furthermore, in the optimized acidic environment, the side reactions were suppressed, so dopaquinone can be changed favorably to quinone methide, which is more easily attacked by nucleophiles through the 1,4-Michael addition (Fig. 1b). This led to a high reaction efficiency and was represented by the smooth and even layer formation within a short time.

Next, the mediator- and GOx-modified electrode was dipped in 50% PPS for protection and dried at room temperature for 1 h; it was then recoated with 30% PPS and dried at room temperature for 12 h. Finally, we developed the CGMS sensor module for practical use (Fig. 1d). The transmitter consisted of a micro controller unit (MCU; STM32F411; STMicro, Switzerland), a miniaturized potentiostat, an analog to digital converter module (ADS1222; Texas Instruments, USA), a Bluetooth and near-field communication (NFC) module, and a flexible lithium-ion polymer battery (FLPB253030R; Routejade, Korea). The potentiostat applies a specific working potential to the glucose sensor and measures the current generated by glucose oxidation. The acquired analog data are amplified using a trans impedance amplifier (current-to-voltage converter) and digitized by a 24-bit analog-to-digital converter (ADC). The transmitter continuously sends the current values from the sensor to a mobile phone with the 2.4-GHz Bluetooth module (CSR1012; CSR, UK) and can thus provide a hypoglycemia alert to the diabetic patient. Using the NFC (M24LR64; STMicro), the data stored in the transmitter memory can also be transferred to the mobile device, which utilizes 13.56-MHz in ISO15693.

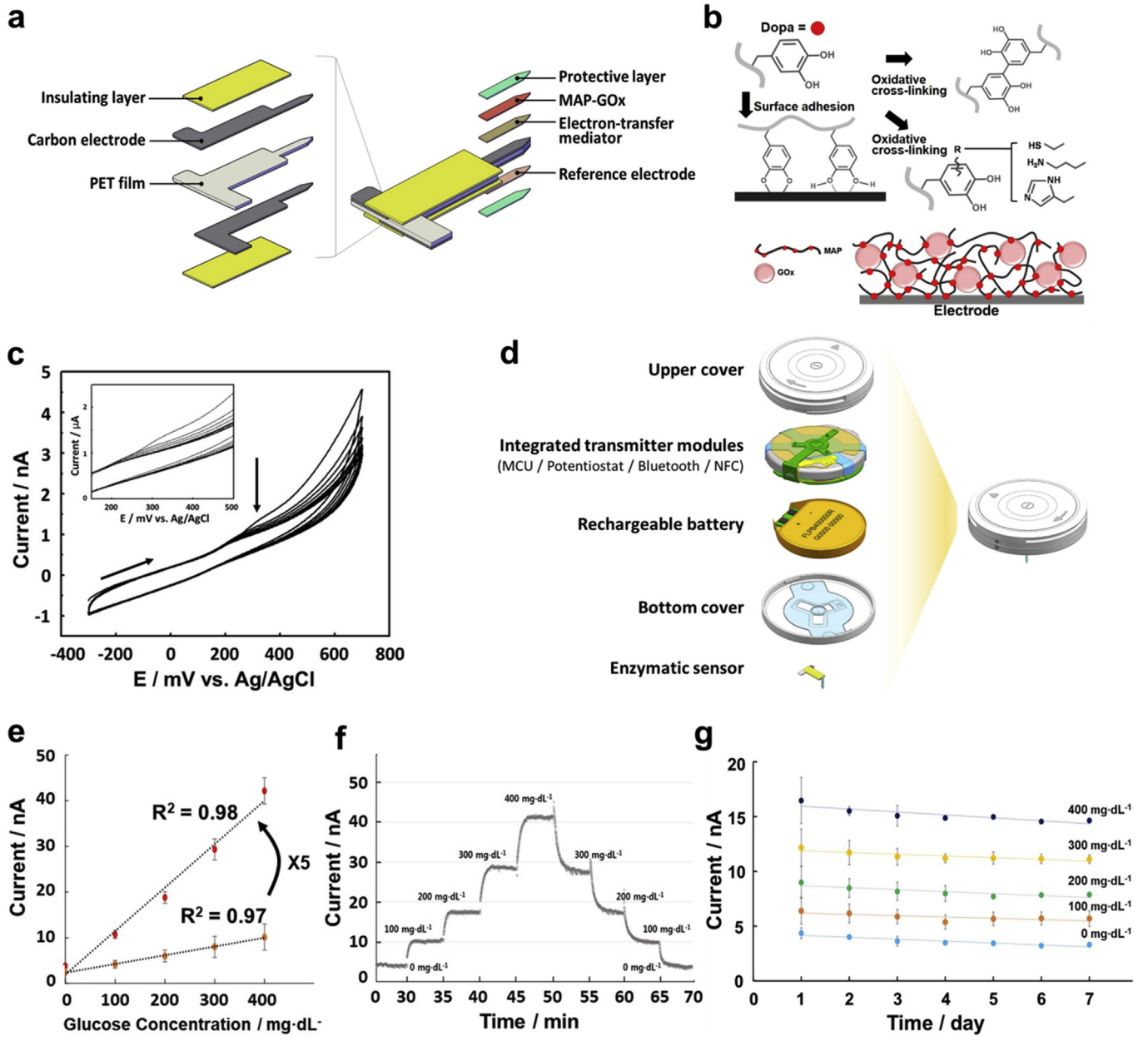

Fig. 1. Fabrication of glucose sensor and its glucose response, long-term stability, and selectivity. (a) The main substrate is the PET film, and the carbon is coated by a silk-screen printer covered with an insulating layer. The sensor materials consisted of a protective layer (PPS), an electron-transfer mediator (FA), immobilized GOx with MAP, and a reference electrode (Ag/AgCl). (b) Schematic representation of the oxidation of Dopa in MAP to conjugate GOx covalently. (c) Cyclic voltammetry for the electrochemical oxidation of the MAP and GOx mixture. (d) A transmitter, consisting of an upper cover with an on/off button, integrated the transmitter modules, the lithium-ion polymer battery, and the bottom cover with the micro-needle. The assembled transmitter was 33 mm in diameter and 7.5 mm in height. (e) Calibration plots for glucose from 0 to 400 mg dL^{-1}. (f) Amperometric current of the sensor for the sequential increase and decrease in the glucose concentration. (g) Long-term stability of the sensor at room temperature for 7 days.

3.2. Glucose response, long-term stability, and selectivity tests

The calibration plot for current versus glucose was obtained by measuring the chronoamperometric responses with 30 mV as the working potential. Our proposed glucose sensor had a sensitivity of 9.57 nA/100 mg dL^{-1} (R^2 = 0.98), which was 5 times higher than a conventional glucose sensor, with a sensitivity of 1.93 nA/100 mg dL^{-1} (R^2 = 0.97) (Fig. 1e). The sensor response time was defined as the time required to reach 90% of the saturation amperometric response for a particular glucose concentration. This parameter is related to the mass transfer barriers that the layers impose on the diffusion of glucose and the enzymatic byproduct (gluconic acid) to attain equilibrium upon a change in the glucose levels (Vaddiraju et al., 2011). The proposed sensor responded well when subjected to sequential increments and decrements of glucose (Fig. 1f). Following each glucose addition step, the sensor response time was approximately 60 s.

The long-term stability of the developed glucose sensor was evaluated over 7 days using five different glucose concentrations (0–400 mg dL^{-1}) daily, and the working potential was decreased from 30 to 10 mV to prolong the stability (Fig. 1g). During the test, the sensor was examined 10 times by exposing it to every glucose concentration, and it was steeped in a 100 mg dL^{-1} glucose standard solution by applying a potential when it was not being tested. Although the magnitude of the error on day 1 was higher than other days, the current

response stabilized after 30 min and showed almost the same values as the initial value within a CV of 4.82%.

The selectivity of the glucose sensor was evaluated with a glucose standard solution in the presences of four major exogenous interfering substances, including ascorbic acid, acetaminophen, dopamine, and uric acid (Fig. S2). These interfering substances have similar oxidation potentials to glucose and can affect the glucose response signal (Rahman et al., 2009). Each interfering species was prepared at 10 mM and diluted to testing concentration with phosphate-buffered saline (PBS; pH 7.4) for the spiking test (Table S1). The interference tests were conducted in accordance with ISO 15197 (Table S2). The variation of the amperometric response of the control and test samples was at an applied potential of 30 mV. From the result, the proposed CGMS sensor had a measuring error under 3%, which was negligible in the accuracy of the glucose sensor (Deng et al., 2014).

3.3. In vivo test with temperature compensation

Because GOx is a protein molecule, the output of the GOx enzyme-based glucose sensor is affected by temperature (Haupt et al., 2005). To find the temperature dependency of the enzyme sensor, the glucose solution (150 mg dL^{-1}) was tested using the proposed glucose sensor at different temperatures from 25 °C to 40 °C. The temperature was measured with the thermistor embedded in the glucose sensor module. The output of the sensor changed from 7.4 mV to 35.1 mV, and the sensor activity was linearly proportional to the temperature with an R-squared of 0.97 (Fig. S3). Therefore, the temperature compensation was highly essential for the enzyme-based sensor to quantify the exact glucose level. To compensate for the temperature effect, it was important to acquire the temperature of the sensing position. We utilized both the skin and the outside temperatures to estimate the temperature of the needle tip-end positioned under the skin. Detailed temperature compensation algorithm was described in the Supporting Information.

To verify our proposed temperature compensation algorithm, the glucose sensor was used on a beagle in different temperature environments (Fig. 2a). The *in vivo* test was approved by Institutional Animal Care and Use Committee (IACUC; ORIENT-IACUC-17047). At the same time, the ambient and skin temperatures were collected for a temperature compensation algorithm. The blood glucose concentration, as a reference value, was measured with an Accu-chek Performa (Roche, Switzerland) at 10-min intervals during continuous glucose monitoring. The raw data were compensated for using two kinds of temperature compensation algorithms, including the conventional algorithm, which used only the skin temperature, and the proposed algorithm, which used both the ambient and skin temperatures. To control the ambient temperature, the experimental beagle was placed in an air-conditioned room at 16 °C, in a room-temperature room, and in a heated room at 45 °C. When the ambient temperature deviated from the normal room temperature (~20–30 °C), the conventional temperature compensation algorithm proceeded with an overcorrection that considered the degradation of the enzyme performance due to the low skin temperature in the air-conditioned room and the hyperactivity of the enzyme performance due to the high skin temperature in the heated room (Fig. 2b). In contrast, because the proposed algorithm estimated the temperature of the sensing tip-end accurately, the compensation was conducted appropriately and considered the enzyme activity accurately. As a consequence, the difference between the reference and the processed data was reduced from 8.3 mg dL^{-1} to 3.6 mg dL^{-1}, on average, and it was a 57% improvement over the conventional algorithm.

3.4. In vivo test with time-lag compensation

CGMS measures the glucose concentration in ISF in the subcutaneous tissue, and the glucose in ISF is diffused across the capillary wall from blood. Therefore, there is a time-lag between the glucose levels in ISF and blood. Specifically, the time-lag is observed obviously during both the rising and decreasing blood glucose levels (Scuffi et al., 2012). Because accuracy is the most important requirement for a CGMS and time-lag is one of the main sources causing the inaccuracy, a time-lag compensation algorithm is necessary to benefit patients in the management of their glucose levels and reduces the risk of hypoglycemia. When the blood glucose levels rise or fall rapidly, the diffusion rate cannot follow the change rate. However, when the blood glucose levels are maintained at a certain level, the diffusion rate sufficiently follows the blood glucose change rate. Therefore, we developed the proposed time-lag compensation algorithm based on the glucose change rate (Fig. S4). Detailed time-lag compensation algorithm was described in the Supporting Information.

To verify our proposed time-lag compensation algorithm, a diabetic cynomolgus monkey was tested with the proposed glucose sensor for 5 days (Fig. 2c). The *in vivo* test was approved by IACUC (ORIENT-IACUC-16304). For the reference values, blood was extracted from the venous capillary, and the blood glucose concentration was measured with Accu-chek Performa at 10- or 15-min intervals. For the glycemic controls, feeding and insulin treatments were conducted. The performance of the time-lag compensation algorithm was evaluated with the degree of synchronization between the reference data and the proposed CGMS data. The synchronization was assessed by the peak-interval between the data sets. Without applying the time-lag compensation algorithm (light blue dots), the average time-lag was 16 min; such a weak synchronization could not reflect the blood glucose trend in real time and could lead to dangerous situations, such as hypoglycemic shock (Fig. 2d). However, as expected, the proposed time-lag compensation algorithm (blue dots) mitigated the average of the time-lag to 5 min, which is sufficient for high accuracy and hypo/hyperglycemic alerts.

3.5. Pre-clinical evaluation of proposed CGMS

Four diabetic beagles participated in the pre-clinical study (ORIENT-IACUC-17047). A diabetic animal model was made by treatment with streptozotocin (STZ), which is particularly toxic to the insulin-producing beta cells of the pancreas in mammals. Before the STZ treatment, the beagles fasted for 16 h. Then, STZ was dissolved with cold excipient, and the STZ solution was injected through the vein of the front leg. Then, 4–6 h after STZ injection, 50% D-glucose subcutaneous administration or 50% glucose solution oral administration was conducted in preparation for hypoglycemic shock.

The sensor was applied on the back between the forelegs of the diabetic beagles with a custom-made inserter, which shod the sensor by a spring force. After the insertion, the sensor-applied part was covered with a bandage for protection. Accu-chek Performa was used as a reference device, and the blood was sampled from the vein in the foreleg using a 26-gauge syringe. A diabetic beagle wearing the proposed CGMS underwent two cycles (one in the morning and the other in the afternoon) per day and 9 total cycles in each 5-day experiment. The test started in the afternoon on the first day and ended in the morning on the fifth day. One cycle was composed of one 50% D-glucose intravenous injection, one insulin treatment and 16 blood samplings. Before the D-glucose injection, 3 blood samplings, at 15-min intervals, were conducted. After the injection, 7 blood samplings, at 10-min intervals for the first hour, and 6 blood samplings, at 15-min intervals for the next hour and a half, were conducted.

Fig. 3a shows one of the representative pre-clinical study results for 5 days. In one test cycle, the blood glucose concentration increased after the 50% D-glucose injection and then decreased due to the insulin treatment. The data from the proposed CGMS were well synchronized with the reference data for the whole experimental period. Overall, the data from the proposed CGMS (light blue dots) had only a 5.72 min time-delay compared to the reference data (red dots) and a MARD of 7.34%, on average, for the 4 preclinical test cases. In addition, we performed a Clarke error grid (CEG) analysis to evaluate the proposed CGMS (Fig. 3b). For all the ranges on the CEG plot, 82.8% of the points

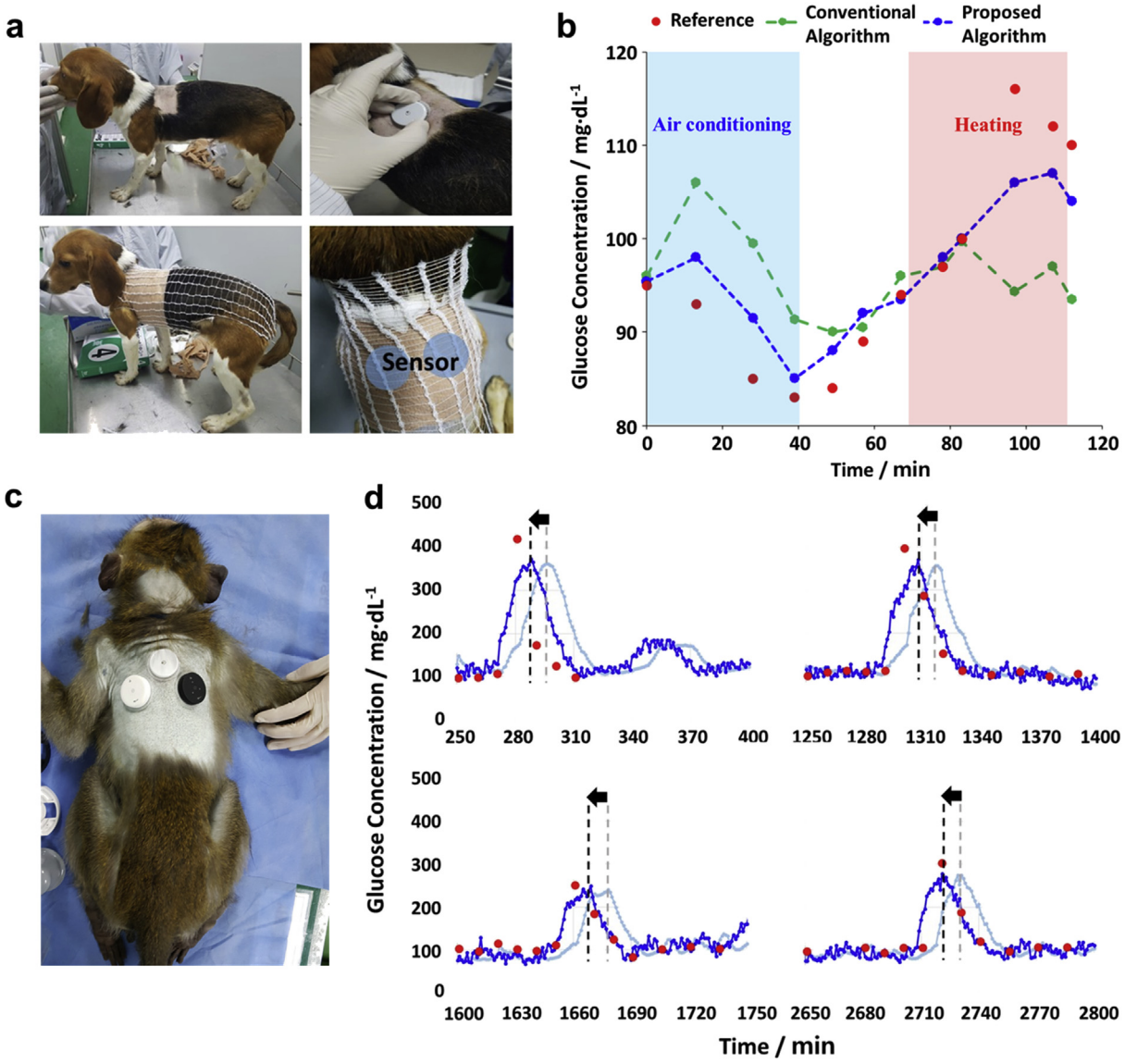

Fig. 2. *In vivo* tests of the developed temperature and time-lag compensation algorithms. (a) Inserting procedures of the sensors on a beagle for testing the temperature compensation algorithm and (b) *in vivo* test results according to the temperature changes in air-conditioned and heated rooms. (c) Inserting sensors on the diabetic cynomolgus monkey for testing the time-lag compensation algorithm and (d) *in vivo* test results of the time-lag reduction. Red dot: reference, light blue dot: proposed CGMS without the algorithm, and blue dot: proposed CGMS with the algorithm. (For interpretation of the references to colour in this figure legend, the reader is referred to the Web version of this article.)

fell in the clinically accurate A zone, with 99.8% of all falling in the A and B zones. In addition, 0.2% of the points were in the D zone. As a result, we confirmed that the proposed CGMS has a better performance than the commercial CGMS over the whole concentration range (70–400 mg dL^{-1}) (Table 1).

3.6. Pilot-clinical evaluation of proposed CGMS

Ten volunteers (6 males and 4 females between the ages of 24 and 57) with type 1 diabetes were recruited using a research protocol and consent that were approved by the institutional review board (IRB; SMC-2017-06-049-007) at the Samsung Medical Center (SMC) in Seoul, Korea. The volunteers were hospitalized at SMC for three days and were fitted with the proposed CGMS and a heparin lock to obtain the venous blood samples (Fig. 4a). After stabilizing the sensor on the first day, an oral glucose tolerance test (OGTT) and a meal tolerance test (MTT) proceeded during the trial period. The subjected drank the oral glucose Diasol-S solution (Taejoon Pharm, Korea) within 5 min instead of breakfast for the OGTT. The glucose data from the CGMS were obtained every 60 s, and the venous blood samples were collected once before the OGTT, 5 times every 15 min from 0 to 60 min after the OGTT, and 6 times every 20 min until 120 min after the OGTT. At lunchtime, an MTT was performed after the intake of the standardized meal provided by the institution. Blood sampling was performed once before the MTT, 5 times every 15 min between 0 and 60 min after the MTT, and 6 times every 20 min for 120 min. The glucose levels in the collected blood samples were measured on a YSI 2300 STAT Plus (Yellow Springs Instruments, USA) which is accepted as a golden standard, and the data were used as reference values for evaluating the accuracy of the proposed CGMS. We found that there was no any swelling or rash developed after insertion of the sensor needle (data not shown). While we observed some reddish traces on the skin of a few volunteers due to prolonged sensor attachment, those disappeared within 3 days after the tests.

Fig. 4b shows 420 paired glucose measurements from the proposed CGMS and YSI 2300, which are plotted on CEG scatter plots to

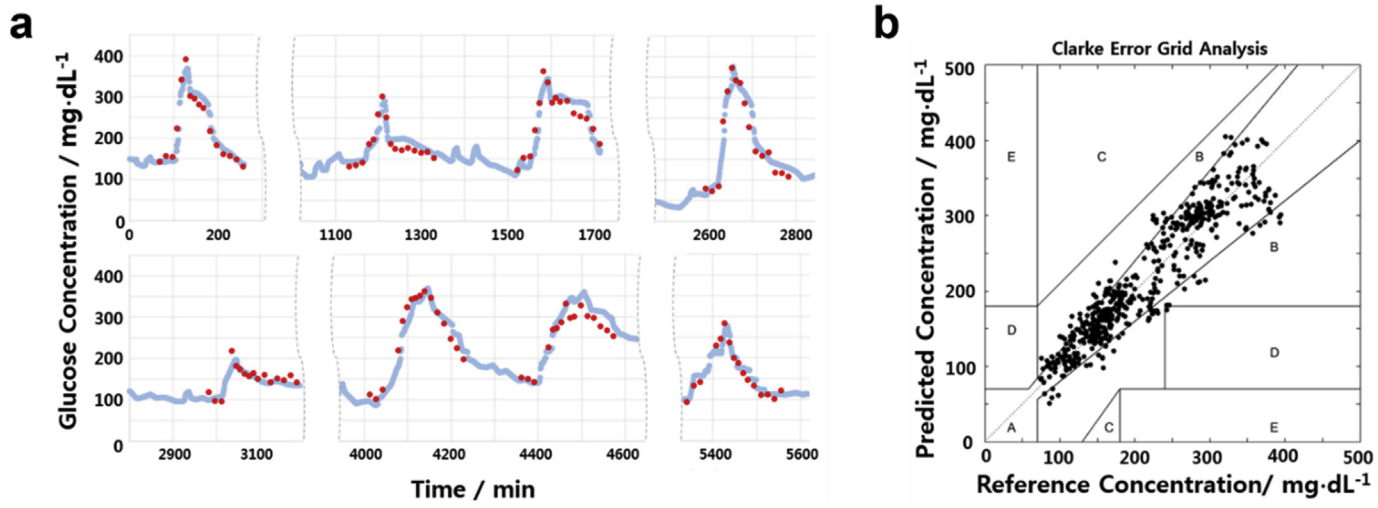

Fig. 3. Pre-clinical evaluation of the proposed CGMS (a) Representative pre-clinical test results for 5 days. Red dot: reference, light blue dot: proposed CGMS. (b) CER analysis results for the pre-clinical tests with 4 diabetic beagles. (For interpretation of the references to colour in this figure legend, the reader is referred to the Web version of this article.)

Table 1
Comparisons of the CEG analysis results with several commercial CGMSs.

Product	N	MARD (%)	Clarke Error Grid Zones (%)						FDA approved
			A + B	A zone	B zone	C zone	D zone	E zone	
Proposed CGMS (this work)	420	7.3	99.8	82.8	17.0	0.0	0.2	0.0	
Abbott Freestyle Navigator	20362	12.8	98.3	81.7	16.7	0.1	1.6	0.0	2008
Medtronic Minimed Guardian RT	3941	19.0	96.0	61.7	34.4	0.2	3.5	0.2	2005
Medtronic Minimed 670G	12090	10.6	–	–	–	–	–	–	2016
Dexcom G4	1477	12.6	97.2	77.9	19.3	0.0	2.8	0.0	2012
Dexcom G4 Platinum w/Software 505	2263	9.0	99.5	92.4	7.1	–	–	–	2014

determine whether the developed CGMS can be used to provide clinically useful glucose values. As shown in the inset, 94.05% of the measurements fell in the A zone, with 99.7% of all measurements falling in the A and B zones. Only one point was in the D zone, and not a single value fell in either the C or E zone. The accuracy of the CGMS was also assessed using MARD, which indicated how closely the proposed CGMS results and the reference values matched. The aggregate MARD for our CGMS was 7.49%, based on the individual paired data points (Table S3). Collectively, according to the results from pilot-clinical trials, the proposed CGMS was sufficient to manage the blood glucose level by monitoring the trend of the blood glucose changes and detecting hypoglycemia/hyperglycemia with a better performance than the conventional CGMS.

4. Conclusion

In this work, we proposed a novel CGMS with a MAP-employing enzymatic glucose sensor to enhance the long-term stability and

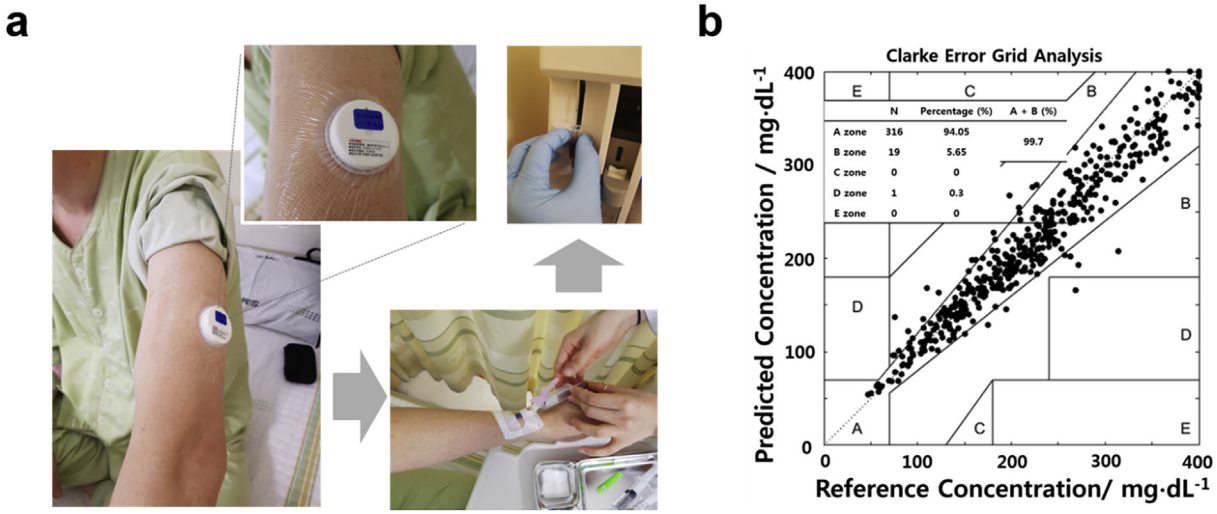

Fig. 4. Pilot-clinical evaluation of the proposed CGMS. (a) Fitting images of the proposed CGMS and the heparin lock. (b) CER analysis for 10 volunteers comprising 420 data pairs.

developed real-time algorithms to compensate both temperature and time-lag differences. First, we proposed innovative approaches using MAP to immobilize the GOx enzyme without loss for long-term use. Thus, the mixture of the GOx and MAP was electrochemically oxidized on the electrode. We confirmed that the proposed glucose sensor with the electrochemically oxidized-MAP had a sensitivity of 9.57 nA/100 mg dL^{-1} which was 5 times higher than that observed for conventional methods. In addition, we demonstrated that the proposed sensor maintained stable outputs with a CV of 4.82% over the entire concentration range (100–400 mg dL^{-1}) for 7 days through *in vitro* tests. Therefore, we proved that the proposed glucose sensor could be used as a CGMS, which requires long-term use. Second, we developed algorithm to compensate for the temperature of the sensing tip-end. Through evaluation of the proposed algorithm-embedded glucose sensor using a beagle in different temperature environments, we confirmed that the proposed algorithm compensated for the temperature effect, with a difference of 3.6 mg dL^{-1} from the reference data, even in an air-conditioned room and a heated room, which was a 57% improvement over the conventional method that used the skin temperature alone. Third, time-lag compensation algorithm was developed to correct the time-lag due to the diffusion from blood to ISF. Through testing the glucose sensor with the proposed algorithm using a diabetic cynomolgus monkey, we confirmed that the proposed algorithm decreased the time-lag from 16 min to 5 min. Next, we conducted preclinical tests using 4 diabetic beagles for 5 days and confirmed that the developed CGMS, with the proposed sensor and the algorithms, followed the blood glucose concentration trends with a MARD of 7.34%, which was similar to that achieved by the disposable glucose meter. In addition, on the CEG plot, 82.8% of all the data were in the clinically accurate A zone, 17.0% were in the B zone, and only 0.2% were in the D zone over the whole range. Finally, the proposed CGMS was tested on human volunteers by the OGTT and MTT protocols. The pilot-clinical trials demonstrated that the proposed CGMS successfully measured the glucose levels in ISF and maintained a high accuracy with a MARD of 7.49%; 99.7% of all measurements fell in the CEG A and B zones. We believe that this is the first work to show that the proposed minimally invasive CGMS using MAP and the accompanying real-time compensation algorithms achieved a performance that was comparable to that of disposable glucose meters.

CRediT authorship contribution statement

Kwang Bok Kim: Writing - original draft. **Hyoungseon Choi:** Writing - original draft. **Hyun Joo Jung:** Methodology. **Young-Jae Oh:** Investigation. **Chul-Ho Cho:** Formal analysis. **Jin Hong Min:** Formal analysis. **Seoyoung Yoon:** Validation. **Jaepil Kim:** Formal analysis. **Seong Je Cho:** Writing - original draft. **Hyung Joon Cha:** Writing - original draft.

Declaration of competing interest

The authors declare that they have no known competing financial interests or personal relationships that could have appeared to influence the work reported in this paper.

Acknowledgements

Financial support was provided by the Samsung Electronics grant from Samsung Research (RAJ0117ZZ-01RF).

Appendix A. Supplementary data

Supplementary data to this article can be found online at https://doi.org/10.1016/j.bios.2019.111622.

References

Atta, N.F., Galal, A., Wassel, A.A., Ibrahim, A.H., 2012. Int. J. Electrochem. Sci. 7, 10501–10518.
Bartlett, P.N., Blrkln, P.R., 1994. Anal. Chem. 66, 1552–1559.
Battaglinit, F., Calvo, E.J., 1994. J. Chem. Soc., Faraday Trans. 90, 987–995.
Carr, P.W., Browers, L.D., 1980. Immobilized Enzyme in Analytical and Clinical Chemistry. Wiley, NY, USA.
Cass, A.E., Davis, G., Francis, G.D., Hill, H.A., Aston, W.J., Higgins, I.J., Plotkin, E.V., Scott, L.D., Turner, A.P., 1984. Anal. Chem. 56, 667–671.
Cha, H.J., Hwang, D.S., Lim, S., 2008. Biotechnol. J. 3, 634–638.
Chao, C., Liu, J., Wang, J., Zhang, Y., Zhang, B., Zhang, Y., Xiang, X., Chen, R., 2013. ACS Appl. Mater. Interfaces 5, 10559–10564.
Deng, H., Teo, A.K.L., Gao, Z., 2014. Sens. Actuators B Chem. 191, 522–528.
Guillod, L., Comte-Perret, S., Monbaron, D., Gaillard, R.C., Ruiz, J., 2007. Diabetes Metab. 33, 360–365.
Hamad, K., Haojie, Y., Wang, L., Wael, A.A., Muhammad, A., Nasir, M.A., Zain ul, A., Muhammad, S., 2014. Polym. Chem. 5, 6879–6892.
Harkness, J.K., Murphy, O.J., Hitchens, G.D., 1993. Electroanal. Chem. 357, 261–272.
Haupt, A., Berg, B., Paschen, P., Dreyer, M., Häring, H.U., Smedegaard, J., Matthaei, S., 2005. Diabetes Technol. Ther. 7, 597–601.
Ishihara, K., Shibata, N., Tanaka, S., Iwasaki, Y., Kurosaki, T., Nakabayashi, N., 1996. J. Biomed. Mater. Res. A. 32, 401–408.
Lee, H., Dellatore, S.M., Miller, W.M., Messersmith, P.B., 2007. Science 318, 426–430.
Lee, H., Rho, J., Messersmith, P.B., 2009. Adv. Mater. 21, 431–434.
Linke, B., Kerner, W., Kiwit, M., Pishko, M., HeIIer, A., 1994. Biosens. Bioelectron. 9, 151–158.
Lion-Dagan, M., Katz, E., Willner, I., 1994. J. Am. Chem. Soc. 116, 7913–7914.
Maleki, A., Nematollahi, D., Clausmeyer, J., Henig, J., Plumeré, N., Schuhmann, W., 2012. Electroanalysis 24, 1932–1936.
NIRAJ, Gupta, M.M., Varshney, H.M., Pandey, S., Singh, S., 2012. Inter. J. Ther. Appl. 6, 28–37.
Rahman, M.M., Umar, A., Sawada, K., 2009. Sens. Actuators B Chem. 137, 327–333.
Rebrin, K., Steil, G.M., 2000. Diabetes Technol. Ther. 2, 461–472.
Rodbard, D., 2016. Diabetes Technol. Ther. 18 (Suppl. 2–13).
Schmelzeisen-Redeker, G., Schoemaker, M., Kirchsteiger, H., Freckmann, G., Heinemann, L., del Re, L., 2015. J. Diabetes Sci. Technol. 9, 1006–1015.
Schmidt, H.L., Gutberlet, F., Schuhmann, W., 1993. Sens. Actuators B Chem. 13, 366–371.
Scuffi, C., Lucarelli, F., Valgimigli, F., 2012. J. Diabetes Sci. Technol. 6, 1383–1391.
Shi, Y., Hu, F.B., 2014. Lancet 383, 1947–1948.
Singh, J., Verma, N., 2013. Adv. Appl. Sci. Res. 4, 250–257.
Sinha, M., McKeon, K.M., Parker, S., Goergen, L.G., Zheng, H., El-Khatib, F.H., Russell, S.J., 2017. J. Dia. Sci. Technol. 11, 1–6.
Steil, G.M., Rebrin, K., Hariri, F., Jinagonda, S., Tadros, S., Darwin, C., Saad, M.F., 2005. Diabetologia 48, 1833–1840.
Stout, P.J., Racchini, J.R., Hilgers, M.E., 2004. Diabetes Technol. Ther. 6, 635–644.
Suri, J.T., Cordes, D.B., Cappuccio, F.E., Wessling, R.A., Singaram, B., 2003. Angew. Chem. Int. Ed. 42, 5857–5859.
Szasz, G., 1974. Z. Klin. Chem. Klin. Biochem. 12, 166–170.
Vaddiraju, S., Legassey, A., Wang, Y., Qiang, L., Burgess, D.J., Jain, F., Papadimitrakopoulos, F., 2011. J. Dia. Sci. Technol. 5, 1044–1051.
Vashist, S.K., 2013. Diagnostics 3, 385–412.
Whiting, D.R., Guariguata, L., Weil, C., Shaw, J., 2011. Diabetes Res. Clin. Pract. 94, 311–321.
Xi, Z., Xu, Y., Zhu, L., Wang, Y., Zhu, B., 2009. J. Membr. Sci. 327, 244–253.
Yang, B., Ayyadurai, N., Yun, H., Choi, Y.S., Hwang, B.H., Huang, J., Lu, Q., Zeng, H., Cha, H.J., 2014. Angew. Chem. Int. Ed. 126, 13578–13582.
Yang, B., Lim, C., Hwang, D.S., Cha, H.J., 2016. Chem. Mater. 28, 7982–7989.
Yang, Y., Zhang, S.F., Kingston, M.A., Jones, G., Wright, G., Spencer, S.A., 2000. Biosens. Bioelectron. 15, 221–227.
Yoneyama, H., Kajiya, Y., 1993. Sens. Actuators B Chem. 13, 65–67.
Yu, J., Wei, W., Danner, E., Ashley, R.K., Israelachvili, J.N., Waite, J.H., 2011. Nat. Chem. Biol. 7, 588–590.
Zhang, Y., Genga, X., Ai, J., Gao, Q., Qi, H., Zhang, C., 2015. Sens. Actuators B Chem. 221, 1535–1541.